Angewandte Chemie

GDCh

Eine Zeitschrift der Gesellschaft Deutscher Chemiker

www.angewandte.de

Akzeptierter Artikel

Titel: Schottky Catalysts Boost Hydrogen Evolution: the Case of MoB/g-C3N4 Interface Materials

Autoren: Zechao Zhuang, Yong Li, Zilan Li, Fan Lv, Zhiquan Lang, Kangning Zhao, Liang Zhou, Lyudmila Moskaleva, Shaojun Guo, and Liqiang Mai

Zitierweise: *Angew. Chem. Int. Ed.* 10.1002/anie.201708748
Angew. Chem. 10.1002/ange.201708748

Link zur VoR: http://dx.doi.org/10.1002/anie.201708748
http://dx.doi.org/10.1002/ange.201708748

WILEY-VCH

10.1002/ange.201708748

WILEY-VCH

Schottky Catalysts Boost Hydrogen Evolution: the Case of MoB/*g*-C_3N_4 Interface Materials

Zechao Zhuang, *Yong Li*, *Zilan Li*, *Fan Lv, Zhiquan Lang*, *Kangning Zhao*, *Liang Zhou*, *Lyudmila Moskaleva**, *Shaojun Guo,* and Liqiang Mai**

Abstract: Moderate proton adsorption on metallic catalysts is a prerequisite for efficient hydrogen evolution reaction (HER). However, precisely tuning the proton adsorption without perturbing metallicity still remains a formidable challenge. Herein, we fabricate an ingenious Schottky catalyst based on metalï semiconductor junction principles. When selecting metallic MoB as a paradigm, the introduction of *n*-type semiconductive *g*-C_3N_4 induces a vigorous charge transfer across the MoB/*g*-C_3N_4 Schottky junction, and increases the local electron density in MoB surface, proved by multiple spectroscopic techniques. This Schottky catalyst exhibits a superior HER activity with a low Tafel slope of 46 mV dec^{-1} and a high exchange current density of 17 εA cm^{-2}, far better than that of pristine MoB. First-principle calculations reveal that Schottky contact dramatically lowers the kinetic barriers of both proton adsorption and reduction coordinates, therefore benefiting the surface hydrogen generation.

Hydrogen is undeniably pursued as one of the most promising green energy carriers to meet the sustainability imperatives.[1] Molybdenum-based electrocatalysts (such as MoS_2, Mo_2C, MoO_2, MoP, and MoB) are emerging as a promising class of noble metal-free catalysts for HER in both acid and alkaline media.[2] Strongly dependent on their electron and phonon structures, Mo-based catalysts exhibit a moderate ñPt-likeò hydrogen binding energy on catalytic centers and a metallic-like transport nature in solid.[3] Thus, it is widely accepted that further optimization of their catalytic performance lies in more precise tuning of the electron and phonon behaviors.[3,4] Many advances have been reported during the last decade, including creating vacancies,[3c,5] phase transformation,[3b,4a,6] or band engineering,[4b,7] which successfully endow additional active sites to Mo-based catalysts for boosting HER catalysis. However, these tactics often inevitably alter the electron transport property at the same time. In particular, the excessively introduced defects may disorder the primitive lattice and induce the anisotropic scattering of phonons, leading to sharp decreases in electron transport efficiency and loss of activity.[3c,8] Given this, an effective strategy for catalyst surface modulation without perturbing interior conductivity is required urgently.

Schottky junction, formed at metalï semiconductor interface, is usually introduced to generate the built-in electric field and enhance the charge separation and transportation for the operation of many semiconductor devices. The difference in Fermi levels between metal and semiconductor sides drives the charge flow propagated by electrons or holes until the system reaches equilibrium, followed by band bending and Schottky barrier formation (**Figure 1**). Rational selection of a semiconductor with suitable majority-carrier type and band structure to build a delicate Schottky junction can adjust the surface charge density of metallic catalyst for specific catalytic reactions.[9,10] For cathodic HER, a metallic surface with enriched electron density could lead to the stabilization of adsorbed hydrogen and catalytic activity enhancement.[2,3] In this regard, designing an ingenious Mo-based Schottky catalyst to achieve more efficient HER, without introducing new lattice defects, is highly desirable, but still waiting to be developed.

Herein, we report a MoB/*g*-C_3N_4 Schottky catalyst with remarkable HER activity enhancement by inducing the charge redistribution across a Schottky contact with an *n*-type semiconductor. Tetragonal *Ŭ*-MoB, displaying intrinsic metallicity, is chosen as our paradigm, and proposed as an alternative HER catalyst (yielding Tafel slopes of ~60 mV dec^{-1}).[2f,2g,11] We utilize an *n*-type *g*-C_3N_4 with a wide band gap of 2.7 eV as the semiconductor side. The Fermi level of *g*-C_3N_4 outbalances substantially all metals, and makes itself available for Schottky contact formation.[12] A series of MoB/*g*-C_3N_4 Schottky catalysts with diverse charge transfer states were simply constructed by proportionally blending two components. Expectedly, the optimal Schottky catalyst exhibits an outstanding and stable performance with a Tafel slope of 46 mV dec^{-1} and an exchange current density of 17 εA cm^{-2}, far better than that of pristine MoB. Such a synergistic optimization is clearly understood *via* integrating spectroscopic evidences with theory computations. This study embraces the band theory and provides an accessible method to activate metallic Mo-based catalysts.

Figure 2a shows the X-ray diffraction (XRD) pattern of commercial MoB. It can be indexed to a tetragonal structure in space group $I4_1/amd$ (Z = 8), in which alternate zigzag chains of boron atoms align along the [100] and [010] crystallographic directions, and each boron chain is enclosed by hexagonal molybdenum atoms (*inset* of **Figure 2a**). A metallic temperature-dependent resistivity for MoB is observed as anticipated (**Figure 2b**), manifesting an increase of resistance in signal with increasing temperature within the whole measured range of 20ï 300 K. Density functional theory (DFT) calculation also reveals the intrinsic metallicity of MoB with large local density of states (DOS) across the Fermi level (**Figure S1**). The XRD pattern of as-prepared *g*-C_3N_4 in **Figure 2c** displays two typical (100) and (002) diffraction peaks, providing a solid evidence for the successful formation of

[*] Z. Zhuang,[+] Z. Li,[+] Z. Lang, K. Zhao, Prof. L. Zhou, Prof. L. Mai
State Key Laboratory of Advanced Technology for Materials Synthesis and Processing, International School of Materials Science and Engineering, Wuhan University of Technology, Wuhan 430070, China
E-mail: mlq518@whut.edu.cn
F. Lv, Prof. S. Guo
Department of Materials Science and Engineering, College of Engineering, Peking University, Beijing 100871, China
E-mail: guosj@pku.edu.cn
Y. Li,[+] Dr. L. Moskaleva
Institute of Applied and Physical Chemistry and Center for Environmental Research and Sustainable Technology, Universität Bremen, Bremen 28359, Germany
E-mail: moskaleva@uni-bremen.de
Dr. L. Mai
Department of Chemistry, University of California, Berkeley, California 94720, United States
[+] These authors contributed equally to this work and should be considered as co-first authors.
Supporting information for this article is given via a link at the end of the document.

10.1002/ange.201708748

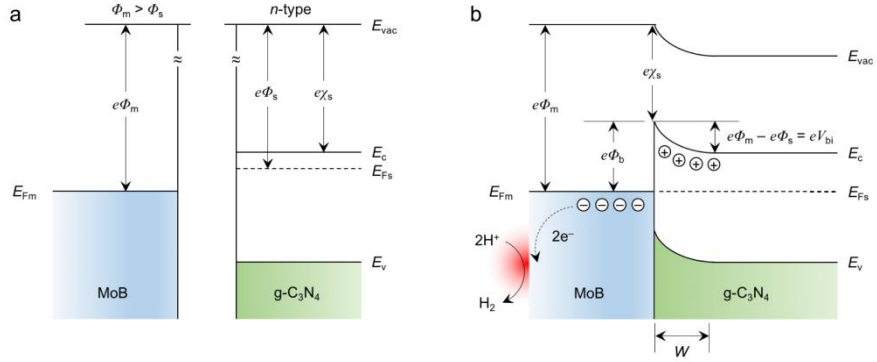

Figure 1. Energy band diagrams of metallic MoB and *n*-type semiconductive *g*-C_3N_4 before (a) and after Schottky contact (b). E_{vac}: vacuum energy; E_c: conduction band; E_v: valence band; E_F: Fermi level; $\bar{u}$: vacuum electrostatic potential; χ: vacuum ionization energy; V: electric potential; e: electric charge; W: depletion region.

g-C_3N_4.The C/N molar ratio is close to the theoretical value of ~0.75, determined by X-ray photoelectron spectroscopy (XPS) and elemental combustion analysis (**Figure S2**). The bandgap energy of *g*-C_3N_4 is further calculated to be ~2.7 eV using Kubelka-Munk remission function (**Figure 2d** and its *inset*), being in accordance with the previous reports.[12,13] In order to fabricate an effective Schottky junction (**Figure 1**), the proportional quantities of both samples were mixed and ground. The scanning electron microscopy (SEM) and transmission electron microscopy (TEM) images of the mixture, coupled with energy-dispersive spectroscopy (EDS) elemental mapping, demonstrate that the Mo, B, C, and N signals spatially correlate with each other, indicating the close mutual contacts between the powder samples (**Figure S3** and **S4**). Meanwhile, the crystallinity of MoB and *g*-C_3N_4 after mixing remains unchanged, and no contamination was introduced (**Figure S5**).

The HER activities of MoB, *g*-C_3N_4, and MoB/*g*-C_3N_4 Schottky catalysts were examined in N_2-saturated 1 M KOH solution. The linear sweep voltammetry (LSV) curve of the pristine MoB shows an onset overpotential of ~80 mV (**Figure 3a**), while the semiconductive *g*-C_3N_4 does not show an obvious HER activity (**Figure S6**). For MoB/*g*-C_3N_4 Schottky catalyst, its voltammogram presents an obvious shift to a more positive overpotential of ~40 mV, beyond which the cathodic current rises steeply along negative potentials. This Schottky catalyst attains a cathodic current of 20 mA cm^{-2} at the overpotential of 152 mV, whereas the pristine MoB only reaches ~4 mA cm^{-2} under the same condition. The Tafel plots and exchange current densities were also extracted (**Figure 3b** and **Table S1**). The pristine MoB displays a Tafel slope of 58 mV dec^{-1} and an exchange current density of 8 εA cm^{-2}. Rather, the MoB/*g*-C_3N_4 Schottky catalyst shows a far higher HER activity with a lower Tafel slope of 46 mV dec^{-1} and a higher exchange current density of 17 εA cm^{-2}, comparable to, or even exceeding those state-of-the-art noble metal-free catalysts (**Table S1**). Additionally, the Tafel slope of the MoB/*g*-C_3N_4 close to ~40 mV dec^{-1} indicates that electrochemical surface desorption of adsorbed hydrogen, namely Heyrovsky reaction, should strongly control the HER process.[14] The electrochemical impedance spectroscopy (EIS) plots (**Figure S7**) show that the MoB/*g*-C_3N_4 possesses a much smaller R_{ct} than the pristine MoB, indicating a faster HER dynamics involved. The activity of this system shows a volcano-shaped dependence on composition ratios (**Figure 3c**), which illustrates that only an appropriate amount of *g*-C_3N_4 can lead to the maximum synergistic effect. Moreover, a similar trend for activity improvement was also observed in an acid solution (**Figure S6**). Such a trend originates from the fact that introducing excessive inert *g*-C_3N_4 suppresses the positive Schottky effects. In addition, the HER performance observed in alkaline media is higher than that in the acid counterpart. This trend may stem from the fact that the Lewis acidity of boron favors the adsorption of OH$^-$ ions, and the rate-limiting water dissociation of alkaline HER. Furthermore, the effects of carbon Vulcan XC72R and hand grinding on HER activity was further explored. The results further reveal the major factor in enhancing HER activity of MoB/*g*-C_3N_4 is indeed caused by Schottky contact (**Figure S8–S10 and Table S2**).

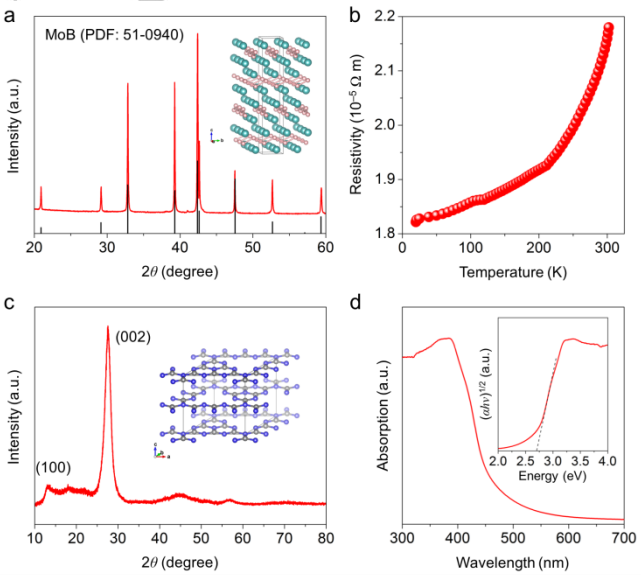

Figure 1. a) XRD pattern and b) temperature-dependent resistivity (ρ T) plots for commercial MoB powders. c) XRD pattern and d) ultraviolet visible (UV vis) analysis for *g*-C_3N_4 powders. Insets show corresponding crystal structures in (a) and (b).

Long-term durability is another key requirement for HER catalysts in industrial applications. The catalysts were analyzed through a chronoamperometric test (**Figure 3d** and **S11**). At a fixed overpotential of 133 mV, the MoB/*g*-C_3N_4 Schottky catalyst yields a stable current density of ~10 mA cm^{-2} over 48 h (**Figure 3d**), similar to the pristine MoB, which also exhibits a stable HER performance but at a much higher overpotential of 183 mV (**Figure S11**). Continuous cyclic voltammetry (CV) was also employed to evaluate the durability of MoB/*g*-C_3N_4. It shows a negligible loss of cathodic current after 5000 cycles, further indicating its high stability for HER (**Figure S12**).

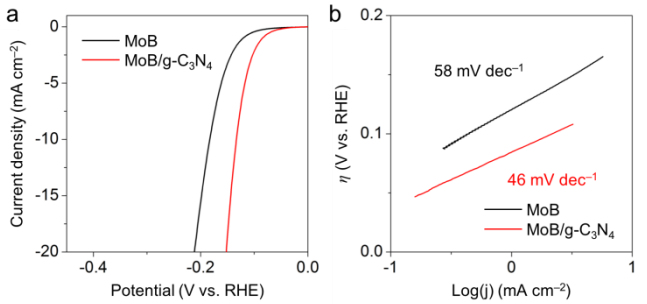

Figure 3. a) LSV polarization curves and b) corresponding Tafel plots. c) A volcano-shaped plot of overpotentials at 5 mA cm^{-2} with respect to MoB/*g*-C_3N_4 Schottky catalysts with different weight ratios. d) Chronoamperometric currentï time (*ïï t*) tests.

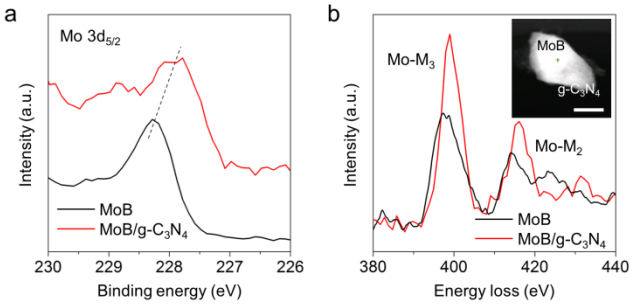

Figure 4. a) Mo $3d_{5/2}$ XPS spectra and b) ELNES of Mo-$M_{2,3}$ edges for pure MoB and MoB/*g*-C_3N_4 Schottky catalyst. c) PL spectra and d) UPS analysis for pure *g*-C_3N_4 and MoB/*g*-C_3N_4 Schottky catalyst. Inset shows corresponding high-angle annular dark field (HAADF) image with green plus indicating the selected region for EELS analysis.

A number of spectroscopic techniques, combined with first-principles simulations, were used to investigate the interfacial interactions and electronic structures of metal and semiconductor before and after Schottky contact. **Figure 4a** shows XPS spectra of MoB and MoB/*g*-C_3N_4. A negative shift (~0.4 eV) of typical Mo $3d_{5/2}$ XPS peaks is observed on MoB/*g*-C_3N_4. And also other Mo XPS peaks, attributed to thin surface oxide, were also shifted negatively on MoB/*g*-C_3N_4 (**Figure S13**). Generally, binding energy negatively correlates with surface electron density.[15] The XPS results suggest that the electrons donated from *g*-C_3N_4 are enriched on the MoB surface. Besides the Mo element, the electron density of B was also increased after Schottky contact with *g*-C_3N_4 (**Figure S14**). The energy-loss near-edge structures (ELNES) spectra of Mo-$M_{2,3}$ edges, which behave sensitively with stimulated 3p electron transitions from spin-orbit-split states to quasi-localized states and reflect the local environment of Mo, are shown in **Figure 4b**. Clearly, the edge-onsets of both the M_3 and M_2 peaks move toward higher energy losses by ~2 eV after Schottky contact (*inset* of **Figure 4b**), implying the alterations in the electronic state of Mo atoms. The M_3/M_2 intensity ratios were found to be 1.5 and 1.8 for MoB and MoB/*g*-C_3N_4, respectively. These ELNES results further support that the Schottky effect creates a fraction of Mo atoms in a reduced state, in decent agreement with the XPS results.

Next, photoluminescence (PL) and ultraviolet photoemission spectroscopy (UPS) were applied to confirm the interface state and band alignments of *g*-C_3N_4. A blue-shifted emission peak was observed in the PL spectrum of the MoB/*g*-C_3N_4 Schottky catalyst (**Figure 4c**), indicating a band gap widening, as the electron depletion causes an upshifting of conduction band edge of *g*-C_3N_4.[16] Further, its PL quenching suggests that the elec-

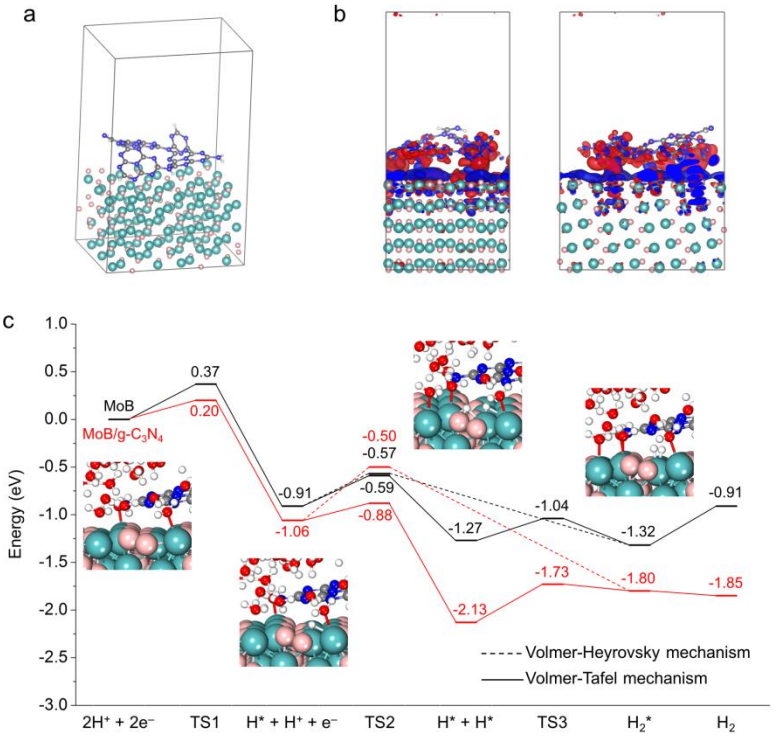

Figure 5. a) Periodic slab model of MoB(112)/*g*-C_3N_4 Schottky catalyst and its b) spatial charge density difference isosurfaces. Blue and red isosurfaces represent electron accumulation and electron depletion, respectively. c) Energy profiles of HER on pure MoB and MoB/*g*-C_3N_4 Schottkycatalyst.

tronī hole pair recombination in the semiconductive g-C_3N_4 is suppressed and thus the charge separation is enhanced[16b] because the excited electrons are readily trapped by metallic MoB. UPS analysis was used to scrutinize the variations in the work function of g-C_3N_4. **Figure 4d** depicts the UPS spectra with the cutoff energy (E_{cutoff}) regions at high binding energies. The E_{cutoff} of g-C_3N_4 and MoB/g-C_3N_4 is 13.9 eV and 13.7 eV, respectively, while the E_f is 0 eV in both cases. The corresponding work functions ($e_{ū}$) can be estimated to be 7.3 eV and 7.5 eV according to the following equation, $e_{ū} = hз ī \mid E_{cutoff} ī E_f \mid$.[17] Such an upshift (~0.2 eV) of the work function validates again the existing Schottky effect. The same conclusion can be further proved by analyzing the spatial charge density difference on a periodic slab model of MoB/g-C_3N_4 (**Figure S15**). As shown in **Figure 5a** and **b**, the charge density of the junction interface is plainly redistributed after the contact between MoB and g-C_3N_4, forming a negatively charged MoB surface and a positively charged g-C_3N_4. This computed geometry corroborates the presence of Schottky junction with vigorous electron transfer from g-C_3N_4 to MoB.

To further provide atomic- and molecular-level understandings, we calculated the detailed energy profiles of HER pathways on bare MoB and MoB/g-C_3N_4 catalysts (**Figure 5c**). Considering that MoB (112) facet has the highest exposure percentage in MoB, we therefore chose this surface as our DFT model example. The strongly coupled Moī B atoms on the MoB surface are well established as the active site,[18] thermodynamically capable of catalyzing the two-electron reduction of two protons to yield dihydrogen. The reaction pathway primarily involves proton adsorption and reduction on the catalyst surface, followed by chemical or electrochemical desorption of the hydrogen molecule. Two possible mechanisms are generally accepted, namely Volmerī Tafel and Volmerī Heyrovsky, to distinguish the different desorption behaviors. For MoB/g-C_3N_4, the overall reaction energies are much lower than those of MoB according to either mechanism. The result demonstrates the higher intrinsic HER activity of this Schottky catalyst and satisfactorily interprets its lower overpotential under a real electrochemical condition. Regarding kinetic barriers, the introduction of g-C_3N_4 lowers the energy barrier for rate-limiting proton adsorption on the MoB by 0.17 eV in the first Volmer step, guaranteeing abundant coverage of adsorbed hydrogen on the catalyst surface for the following steps. If HER further proceeds according to Volmerī Tafel route, the following steps include another proton adsorption and recombination. The second proton can also be easily adsorbed onto the MoB/g-C_3N_4, while the recombination of two protons with a high barrier of 0.40 eV becomes the new rate-limiting step. In the alternative Volmerī Heyrovsky mechanism, the electrochemical desorption step exhibits a higher energy barrier of 0.56 eV, indicating that the HER on the MoB/g-C_3N_4 more likely occurs through a Volmerī Tafel route. This finding seems to be in conflict with the experimental results by Tafel slopes, but the fact should be considered that the use of large and irregular MoB particles may hinder the electron and proton transport during HER, leading to a loss of activity. Therefore, we can expect a better activity through downsizing this Schottky catalyst to compensate the imperfection. From the computational point of view, introducing n-type semiconductive g-C_3N_4 on MoB catalyst indeed creates a situation in which the surface electron density of MoB is enriched such that the proton access to active sites is facilitated, and the reduction kinetic barrier is lowered, significantly boosting the surface hydrogen generation.

In summary, we demonstrate an ingenious strategy to optimize HER catalytic activity of metallic MoB by contacting n-type semiconductive g-C_3N_4 to form a Schottky junction. This Schottky catalyst exhibits a superior and durable HER performance with a Tafel slope of 46 mVdec$^{ī 1}$ and an exchange current density of 17 εA cm$^{ī 2}$, far outperforming the pristine MoB. As revealed by spectroscopic studies, the interface between the MoB and g-C_3N_4 features notable charge redistribution. The activity enhancement can therefore be attributed to the enriched electron density of the MoB surface and to unimpeded electron transfer in the bulk. Computations further validate the lowered kinetic barriers of both proton adsorption and reduction on the Schottky catalyst. This development opens a new avenue for activating metallic electrocatalysts from the band theory of solids.

Acknowledgements

This work was supported by the National Key Research and Development Program of China (2016YFA0202603), the National Basic Research Program of China (2013CB934103), the Programme of Introducing Talents of Discipline to Universities (B17034), the National Natural Science Foundation of China (51521001, 51671003), the National Natural Science Fund for Distinguished Young Scholars (51425204), and the Fundamental Research Funds for the Central Universities (WUT: 2016III001, 2017III009). We thank the North-German Supercomputing Alliance (HLRN) for providing computational resources. Prof. Liqiang Mai gratefully acknowledged financial support from China Scholarship Council (No. 201606955096).

Keywords: Schottky junction Åelectrocatalysis Åhydrogen evolution reaction Åmolybdenum boride Ågraphitic carbon nitride

[1] a) Z. W. Seh, J. Kibsgaard, C. F. Dickens, I. Chorkendorff, J. K. Nørskov, T. F. Jaramillo, *Science* **2017**, *355*, eaad4998; b) L. Lin, W. Zhou, R. Gao, S. Yao, X. Zhang, W. Xu, S. Zheng, Z. Jiang, Q. Yu, Y.-W. Li, et al., *Nature* **2017**, *544*, 80ï 83.

[2] a) J. Kibsgaard, Z. Chen, B. N. Reinecke, T. F. Jaramillo, *Nat. Mater.* **2012**, *11*, 963ï 969; b) W.-F. Chen, C.-H. Wang, K. Sasaki, N. Marinkovic, W. Xu, J. T. Muckerman, Y. Zhu, R. R. Adzic, *Energy Environ. Sci.* **2013**, *6*, 943; c) L. Liao, S. Wang, J. Xiao, X. Bian, Y. Zhang, M. D. Scanlon, X. Hu, Y. Tang, B. Liu, H. H. Girault, *Energy Environ. Sci.* **2014**, *7*, 387ï 392; d) Y. Jin, H. Wang, J. Li, X. Yue, Y. Han, P. K. Shen, Y. Cui, *Adv. Mater.* **2016**, *28*, 3785ï 3790; e) P. Xiao, M. A. Sk, L. Thia, X. Ge, R. J. Lim, J.-Y. Wang, K. H. Lim, X. Wang, *Energy Environ. Sci.* **2014**, *7*, 2624ï 2629; f) H. Vrubel, X. Hu, *Angew. Chemie - Int. Ed.* **2012**, *51*, 12703ï 12706; g) H. Park, A. Encinas, J. P. Scheifers, Y. Zhang, B. P. T. Fokwa, *Angew. Chemie - Int. Ed.* **2017**, 1ï 5; h) X. Zhang, H. Cheng, H. Zhang, *Adv. Mater.* **2017**, *29*, 1701704; i) C. Tan, X. Cao, X.-J. Wu, Q. He, J. Yang, X. Zhang, J. Chen, W. Zhao, S. Han, G.-H. Nam, M. Sindoro, H. Zhang, *Chem. Rev.* **2017**, *117*, 6225ï 6331.

[3] a) T. F. Jaramillo, K. P. Jorgensen, J. Bonde, J. H. Nielsen, S. Horch, I. Chorkendorff, *Science* **2007**, *317*, 100ï 102; b) M. A. Lukowski, A. S. Daniel, F. Meng, A. Forticaux, L. Li, S. Jin, *J. Am. Chem. Soc.* **2013**, *135*, 10274ï 10277; c) H. Li, C. Tsai, A. L. Koh, L. Cai, A. W. Contryman, A. H. Fragapane, J. Zhao, H. S. Han, H. C. Manoharan, F. Abild-Pedersen, et al., *Nat. Mater.* **2016**, *15*, 48ï 53; d) Q. Lu, Y. Yu, Q. Ma, B. Chen, H. Zhang, *Adv. Mater.* **2016**, *28*, 1917ï 1933; e) X. Zhang, Z. Lai, C, Tan, H. Zhang, *Angew. Chemie - Int. Ed.* **2016**, 55, 8816ï 8838.

[4] a) J. Xie, J. Zhang, S. Li, F. Grote, X. Zhang, H. Zhang, R. Wang, Y. Lei, B. Pan, Y. Xie, *J. Am. Chem. Soc.* **2013**, *135*, 17881ï17888; b) J. Wang, M. Yan, K. Zhao, X. Liao, P. Wang, X. Pan, W. Yang, L. Mai, *Adv. Mater.* **2017**, *29*, 1604464; c) H. Wang, Z. Lu, S. Xu, D. Kong, J. J. Cha, G. Zheng, P.-C. Hsu, K. Yan, D. Bradshaw, F. B. Prinz, et al., *Proc. Natl. Acad. Sci.* **2013**, *110*, 19701ï19706; d) C. Wan, Y. N. Regmi, B. M. Leonard, *Angew. Chemie - Int. Ed.* **2014**, *53*, 6407ï6410.

[5] a) H. Li, M. Du, M. J. Mleczko, A. L. Koh, Y. Nishi, E. Pop, A. J. Bard, X. Zheng, *J. Am. Chem. Soc.* **2016**, *138*, 5123ï5129; b) Y. Yin, J. Han, Y. Zhang, X. Zhang, P. Xu, Q. Yuan, L. Samad, X. Wang, Y. Wang, Z. Zhang, et al., *J. Am. Chem. Soc.* **2016**, *138*, 7965ï7972.

[6] K. Chang, X. Hai, H. Pang, H. Zhang, L. Shi, G. Liu, H. Liu, G. Zhao, M. Li, J. Ye, *Adv. Mater.* **2016**, 1ï 9.

[7] D. Voiry, R. Fullon, J. Yang, E. S. C. de Carvalho Castro, R. Kappera, I. Bozkurt, D. Kaplan, M. J. Lagos, P. E. Batson, G. Gupta, et al., *Nat. Mater.* **2016**, *15*, 1003ï 1009.

[8] a) H. P. Komsa, J. Kotakoski, S. Kurasch, O. Lehtinen, U. Kaiser, A. V. Krasheninnikov, *Phys. Rev. Lett.* **2012**, *109*, 035503; b) Y.-C. Lin, D. O. Dumcenco, Y.-S. Huang, K. Suenaga, *Nat. Nanotechnol.* **2014**, *9*, 391ï 396.

[9] a) Y.-Y. Cai, X.-H. Li, Y.-N. Zhang, X. Wei, K.-X. Wang, J.-S. Chen, *Angew. Chemie* **2013**, *125*, 12038ï 12041; b) H. Su, K.-X. Zhang, B. Zhang, H.-H. Wang, Q.-Y. Yu, X.-H. Li, M. Antonietti, J.-S. Chen, *J. Am. Chem. Soc.* **2017**, *139*, 811ï 818.

[10] Z. H. Xue, H. Su, Q. Y. Yu, B. Zhang, H. H. Wang, X. H. Li, J. S. Chen, *Adv. Energy Mater.* **2017**, 1ï 7.

[11] G. Akopov, M. T. Yeung, R. B. Kaner, *Adv. Mater.* **2017**, *29*, 1604506.

[12] Y. Zheng, L. Lin, B. Wang, X. Wang, *Angew. Chemie - Int. Ed.* **2015**, *54*, 12868ï 12884.

[13] H. Wang, S. Jiang, S. Chen, D. Li, X. Zhang, W. Shao, X. Sun, J. Xie, Z. Zhao, Q. Zhang, et al., *Adv. Mater.* **2016**, 6940ï 6945.

[14] a) J. K. Nørskov, T. Bligaard, A. Logadottir, J. R. Kitchin, J. G. Chen, S. Pandelov, U. Stimming, *J. Electrochem. Soc.* **2005**, *152*, J23; b) J. Kibsgaard, C. Tsai, K. Chan, J. D. Benck, J. K. Nørskov, F. Abild-Pedersen, T. F. Jaramillo, *Energy Environ. Sci.* **2015**, *8*, 3022ï 3029.

[15] a) M. Huynh, C. Shi, S. J. L. Billinge, D. G. Nocera, *J. Am. Chem. Soc.* **2015**, *137*, 14887ï 14904; b) C. Kim, H. S. Jeon, T. Eom, M. S. Jee, H. Kim, C. M. Friend, B. K. Min, Y. J. Hwang, *J. Am. Chem. Soc.* **2015**, *137*, 13844ï 13850.

[16] a) Q. Han, B. Wang, Y. Zhao, C. Hu, L. Qu, *Angew. Chemie - Int. Ed.* **2015**, *54*, 11433ï 11437; b) Q. Liang, Z. Li, X. Yu, Z.-H. Huang, F. Kang, Q.-H. Yang, *Adv. Mater.* **2015**, *27*, 4634ï 4639.

[17] J. Liu, Y. Liu, N. Liu, Y. Han, X. Zhang, H. Huang, Y. Lifshitz, S.-T. Lee, J. Zhong, Z. Kang, *Science* **2015**, *347*, 970ï 974.

[18] a) H. Li, P. Wen, Q. Li, C. Dun, J. Xing, C. Lu, S. Adhikari, L. Jiang, D. L. Carroll, S. M. Geyer, *Adv. Energy Mater.* **2017**, *7*, 1700513; b) H. Park, Y. Zhang, J. P. Scheifers, P. R. Jothi, A. Encinas, B. P. T. Fokwa, *J. Am. Chem. Soc.* **2017**, *139*, 12915ï 12918; c) P. R. Jothi, Y. Zhang, J. P. Scheifers, H. Park, B. P. T. Fokwa, *Sust. Energy Fuel* **2017**, *1*, 1928ï 1934.

10.1002/ange.201708748

WILEY-VCH

COMMUNICATION

Schottky catalyst: The hydrogen evolution activity of a metallic MoB catalyst can be significantly promoted by enhancing the surface charge density across a Schottky contact with an *n*-type semiconductor.

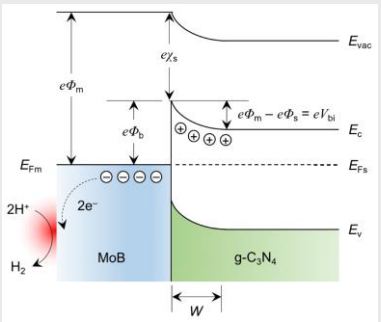

Zechao Zhuang, Yong Li, Zilan Li, Fan Lv, Zhiquan Lang, Kangning Zhao, Liang Zhou, Lyudmila Moskaleva, Shaojun Guo,* and Liqiang Mai**

Page No. – Page No.

Schottky Catalysts Boost Hydrogen Evolution: the Case of MoB/*g*-C_3N_4 Interface Materials